Supporting Information

Accelerated Alkaline Hydrogen Evolution on $M(OH)_x$/M-$MoPO_x$ (M= Ni, Co, Fe, Mn) Electrocatalysts by Coupling Water Dissociation and Hydrogen Ad-Desorption Steps

*Lishan Peng†, Mansheng Liao†, Xingqun Zheng†, Yao Nie, Ling Zhang, Minjie Wang, Rui Xiang, Jian Wang, Li Li, Zidong Wei**

Content:

Experiment and computational details

Figure S1-27

Table S1-6

1. Experiment and computational details

1.1 Experiment and computational details

Synthesis of M(Ni,Co,Fe,Mn)-MoO_4/NF precursors: All chemical reagents used in this experiment were of analytical grade. Prior to the synthesis, the Ni Foam (NF, 50.0 mm×10.0 mm×1.0 mm) was cleaned ultrasonically in a 3.0 mol L^{-1} HCl solution for 15 min to remove the surface oxide layer, and then placed against the wall of a Teflon-lined stainless steel autoclave at a certain angle. Afterwards, 30 mL aqueous solution with 1.50 mol $Ni(NO_3)_2$•$6H_2O$ and 0.22 mol $(NH_4)_6Mo_7O_{24}$•$4H_2O$ was transferred into the above Teflon autoclave. The autoclave was sealed and heated at 150 °C for 6 h. After the hydrothermal reaction was over, the precursors were completely washed with distilled water and dried in an oven at 60 °C. Other M(Ni,Co,Fe,Mn)-MoO_4/NF precursors were synthesized by the same process but changed the $Ni(NO_3)_2$•$6H_2O$ by the corresponding metal nitrates.

Synthesis of M(Ni,Co,Fe,Mn)-$MoPO_x$/NF: The *$NiMoO_4$/NF* precursors with an area of 10 cm^{-2} and 1.2 g NaH_2PO_2 were put in a porcelain boat with a distance of 2 cm and NaH_2PO_2 was placed at the upstream side of the furnace. Then the furnace was heated up to 400 °C with a ramp of 5 °C min^{-1} and stayed for 2 h in the near-static Ar atmosphere. The obtained sample was labelled as *$NiMoPO_x$/NF*, and can be directly used as work electrode. For purposes of comparison, *$NiMoO_4$/NF* were prepared as described above without adding NaH_2PO_2. Other *M(Ni,Co,Fe,Mn)-$MoPO_x$/NF* were synthesized by the same process.

Synthesis of $M(OH)_x$/$MMoPO_x$/NF: The *$NiMoPO_x$/NF* was directly used as work electrode in a three-electrode cell system in 1.0 M NaOH. The electrochemical activation was conducted by CV at -0.3V ~ +0.2V vs. RHE with 100 mV/s for 8000 cycles. The obtained catalytic electrode was named as *$Ni(OH)_2$/$NiMoPO_x$*. All the *M(Ni,Co,Fe,Mn)-$MoPO_x$/NF* were activated by the same process. The *$NiMoPO_x$/NF* activated by different number of CV cycles name as *$NiMoPO_x$*/NF-n CVs*. Without special noted, the sample named *$Ni(OH)_2$/$NiMoPO_x$* means *M(Ni,Co,Fe,Mn)-$MoPO_x$/NF* activated by CV for 8000 cycles. The catalyst loading on the NF is about 1 mg cm^{-1}.

Synthesis of M(Ni,Co,Fe,Mn)-MoP_2/NF: The *$NiMoO_4$/NF* precursors with an area of 10 cm^{-2} and 1.2 g NaH_2PO_2 were put in a porcelain boat with a distance of 2 cm and NaH_2PO_2 was placed at the upstream side of the furnace. Then the furnace was heated up to 650 °C with a ramp of 5 °C min^{-1} and stayed for 2 h in the Ar/H_2 (90/10 sccm) atmosphere. The obtained sample was labelled as *$NiMoP_2$/NF*, and can be directly used as work electrode. Other *M(Ni,Co,Fe,Mn)-$MoPO_x$/NF* were synthesized by the same process.

Synthesis of 20% Pt/C/NF electrode: The commercial Pt/C (20 wt% Pt loading, Johnson Matthey) were prepared by ultrasonically mixing 4 mg of the catalyst powder with the mixture of 40 μL 5% Nafion solution, 560 μL ethanol and 400 μL H_2O for 15 min to form homogeneous catalyst ink. Next, a certain volume of the ink was carefully dropped onto the clean Ni foam, leading to a desirable catalyst loading of about 1.0 mg cm^{-2} (labelled: 20% Pt/C/NF).

1.2 Characterization and electrochemical measurements

The surface morphology and the microstructure of the catalysts were analyzed by X-ray diffraction (XRD-6000, Shimadzu), X-ray photoelectron spectroscopy (XPS, PHI 550 ESCA/SAM), field-emission scanning electron microscopy (FE-SEM, JSM-7800, Japan), and energy dispersive X-ray spectra (EDX, OXFORD Link-ISIS-300), respectively. Electrochemical measurements were conducted in a three-electrode cell system with an Electrochemical Workstation (Auto Lab, Metrohm China Ltd, China). The electrode area of the working electrode is 1.0 cm^2. A carbon rod in parallel orientation to the working electrode was used as the counter electrode and Hg/HgO electrode as the reference electrode. Linear sweep voltammetry (LSV) was performed in N_2 saturated aqueous solution with a scan rate of 5 mV s^{-1}. The long-term durability test was carried out by chronopotentiometry measurements at -100 mV for 90 h. The double layer capacitance of the electrodes was obtained by cyclic voltammetry (CV) from 0.1 to 0.3 V (vs RHE) at scan rate from 2 to 7 mV s^{-1}. The catalytic performance of the prepared electrodes toward HER were systematically investigated in 1.0 M NaOH electrolyte. Electrochemical impedance spectroscopy (EIS) was performed at different over-potentials in the frequency range of 10^5 Hz to 0.01 Hz with a perturbation amplitude of 5 mV. All potentials mentioned in this work were converted to the values with reference to a reversible hydrogen electrode (RHE) via E(RHE) = E(Hg/HgO) + 0.9334 V in 1 M NaOH and all data without *i*R correction unless noted.

The electrolyte (NaOH) used for hydrogen evolution reaction in this work is sourced from Aladdin (99.9%). For rigorously metal impurities-free measurements, the 1 M NaOH electrolyte was purified as follows. In a H_2SO_4-cleaned 50 mL polypropylene centrifuge tube, ~2 g of 99.999% $Ni(NO_3)_2 \cdot 6H_2O$ were dissolved in ~4 mL of 18.2 MΩ·cm H_2O. 20 mL of 1 M NaOH were added to precipitate high-purity $Ni(OH)_2$. The mixture was shaken and centrifuged, and the supernatant was decanted. The $Ni(OH)_2$ then underwent three washing cycles by adding ~20 mL of 18.2 MΩ·cm water and ~2 mL of 1 M NaOH to the tube, re-dispersing the solid, centrifuging, and decanting the supernatant. Finally, the tube was filled with 50 mL of 1 M NaOH for purification. The solid was re-dispersed and mechanically agitated for at least 10 min, followed by at least 3 h of resting. The mixture was centrifuged, and the purified NaOH supernatant was decanted into a H_2SO_4-cleaned polypropylene bottle for storage.

The concentration of PO_3^{3-} dissolved in the electrolyte during electrochemical activation process was detected via phosphomolybdenum blue method using UV-vis-NIR spectroscopy. Typically, 2 mL electrolyte was removed from the cathode chamber and mixed with 2 mL of 0.01 M $(NH_4)_2MoO_4$ solution, followed by the addition of 2 mL of 0.01 M ascorbic acid and 2 mL of 0.5 M H_2SO_4 solution. After incubation at room temperature for 2 h, the UV-vis adsorption spectra with absorbance at ~750 nm was measured using a spectrophotometer.

1.3 Theoretical calculation details

Density functional theory (DFT) calculations were performed by utilizing the Vienna Ab-Initio Simulation Package (VASP) code. The projector augmented wave (PAW) method was used to describe the ionic cores. And the electron exchange-correlation was modelled by Perdew-Burke-Ernzerh of (PBE) function within generalized gradient approximation (GGA). A cut-off

energy of 450 eV was used for the plane-wave basis set. The convergence criterion was 10^{-5} eV for energy and 0.03 eV/Å for force. The Monkhorst−Pack k-point mesh were set to be 3 × 3 × 1 for all systems. To separate adjacent periodic images a 15 Å thick vacuum along the vertical direction was added. In all the structure optimization calculations, the bottom three atomic layers were fixed while other atoms were fully relaxed. Transition states for H_2O dissociation were located using the climbing image-nudged elastic band (CI-NEB) method.

For H adsorption, ΔE_H is hydrogen adsorption energy, and it is defined by: $\Delta E_H = E_{surface+H} - E_{surface} - 1/2E_{H2}$

$E_{surface+H}$ is the total energy of surface with an adsorbed H atom, $E_{surface}$ the energy of surface, E_{H2} is the energy of a gas H_2.

For OH adsorption enrgy: $\Delta E_{OH} = E_{surface+OH} - E_{surface} - E_{OH}$

$E_{surface+OH}$ is the total energy of surface with an adsorbed OH radical, and E_{OH} is the energy of single OH radical.

The Gibbs free reaction energy of hydrogen adsorption ΔG_H was calculated as follow: $\Delta G_H = \Delta E_H + \Delta E_{ZPE} - T\Delta S_H$

Where ΔE_{ZPE} is the difference in zero point energy, and ΔS_H is the difference in entropy between the adsorbed and the gas phase. $\Delta E_{ZPE} - T\Delta S_H$ is about 0.24 eV.

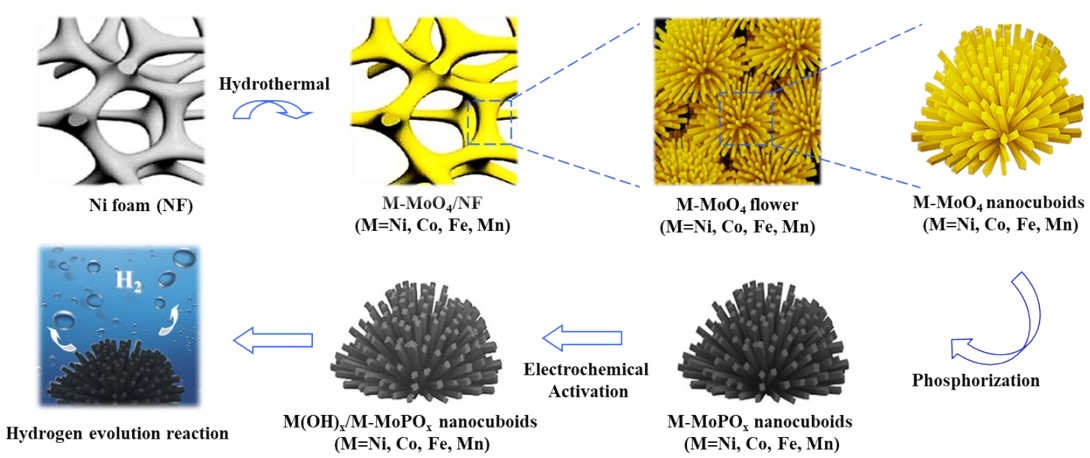

Scheme S1. Schematic illustration of the synthesis processes of M-MoO_4/NF, M-$MoPO_x$/NF and activated $M(OH)_x$/M-$MoPO_x$/NF.

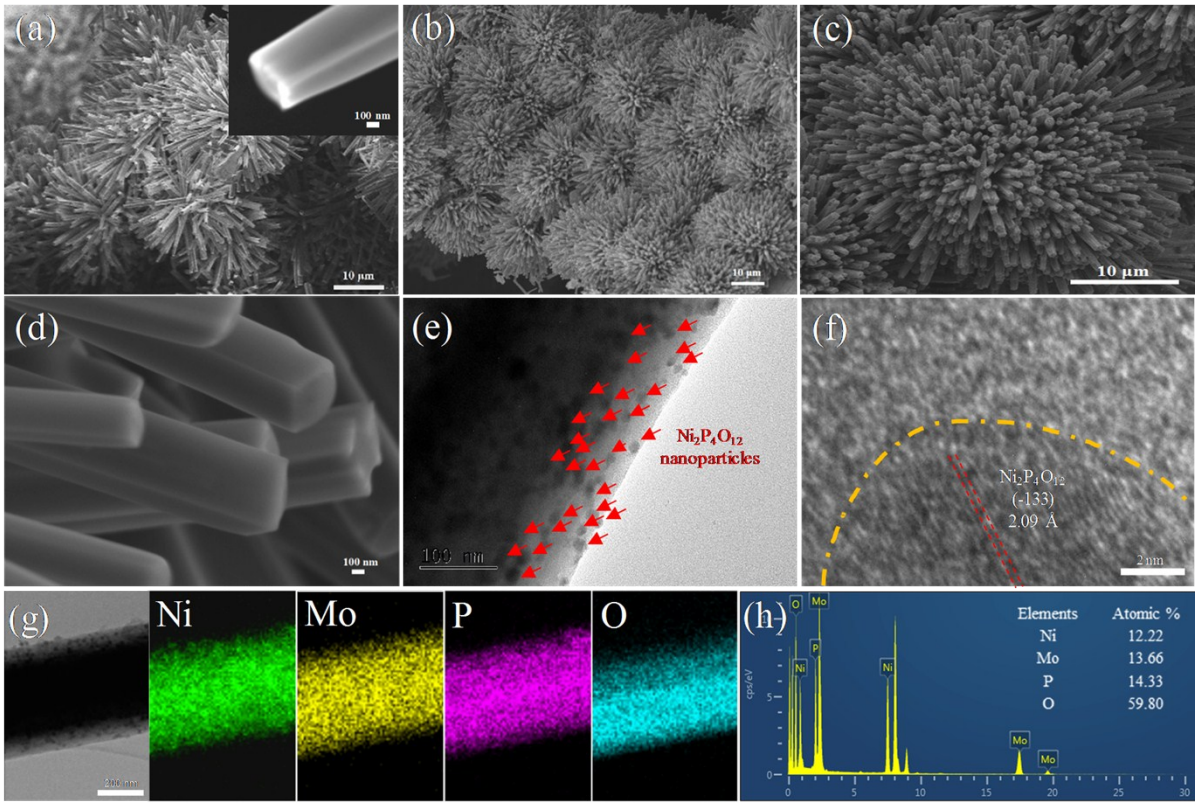

Figure S1. SEM images of (a) $NiMoO_4$/NF, and (b-d) $NiMoPO_x$/NF, inset in (a) is the SEM image of Ni foam. (e) TEM, (f) HR-TEM images, (g) elemental mapping and (h) EDX spectrum of $NiMoPO_x$ powder.

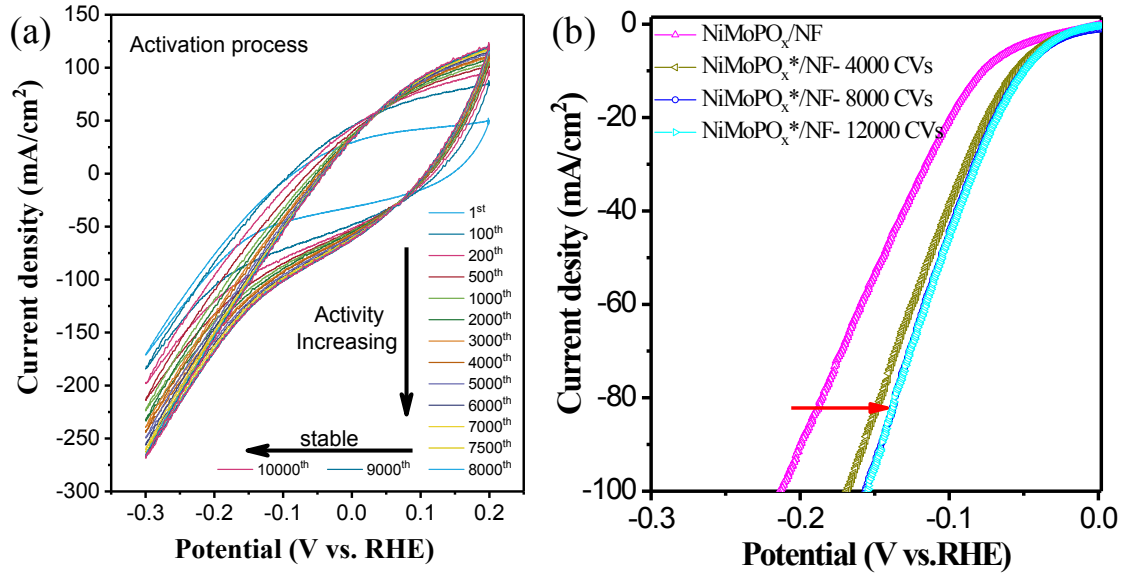

Figure S2. (a) Electrochemical activation of $NiMoPO_x$/NF by CVs, (b) LSV curves of $NiMoPO_x$/NF activated with different CVs without iR correction, (c) XRD patterns of $NiMoO_4$/NF, $NiMoPO_x$/NF, $Ni(OH)_2$/$NiMoPO_x$/NF and Ni foam.

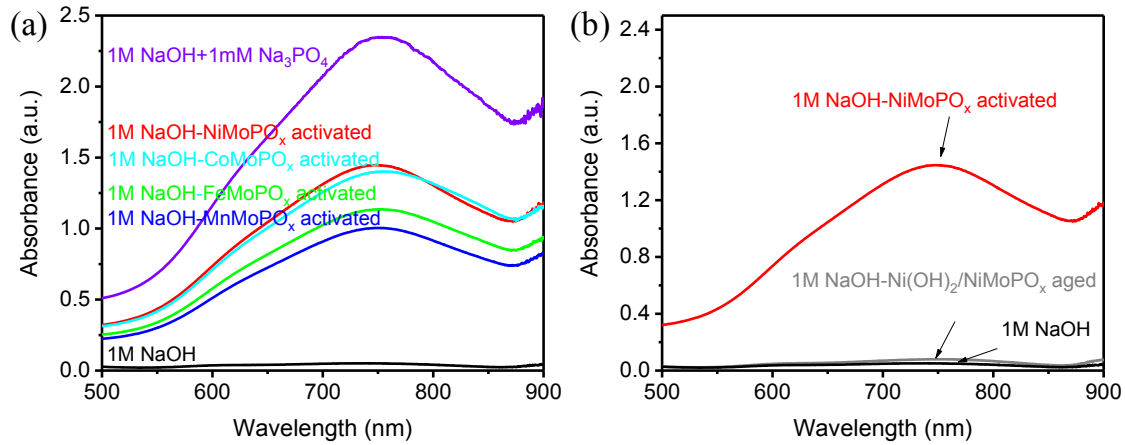

Figure S3. UV-vis absorption spectra of dissolved PO_3^{3-} in (a) M-$MoPO_x$ activated electrolytes and (b) $Ni(OH)_2$/$NiMoPO_x$ aged electrolyte.

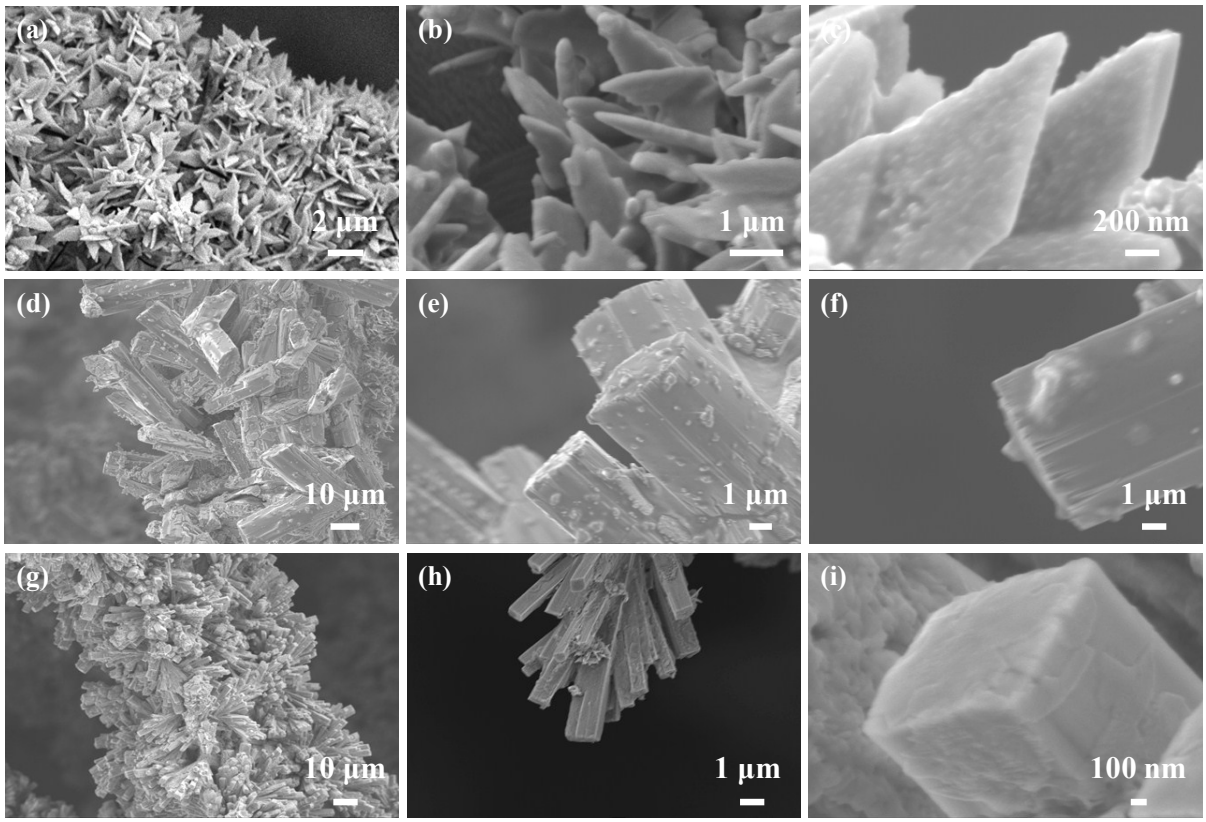

Figure S4. SEM images of (a-c) $FeMoPO_x$/NF, (d-f) $MnMoPO_x$/NF, (g-i) $CoMoPO_x$/NF electrodes.

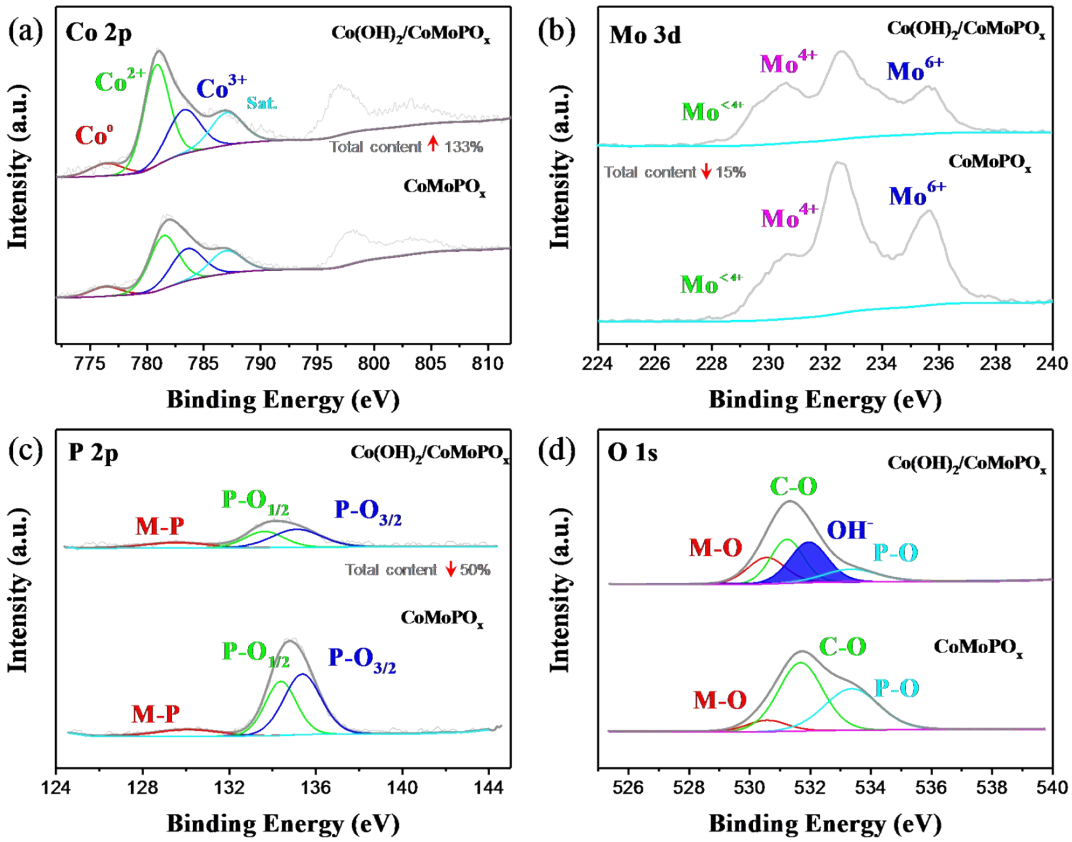

Figure S5. XPS spectra of $CoMoPO_4$, and $Co(OH)_2/CoMoPO_x$, (a) Co 2p region, (b) Mo 3d region, (c) P 2p region and (d) O 1s region.

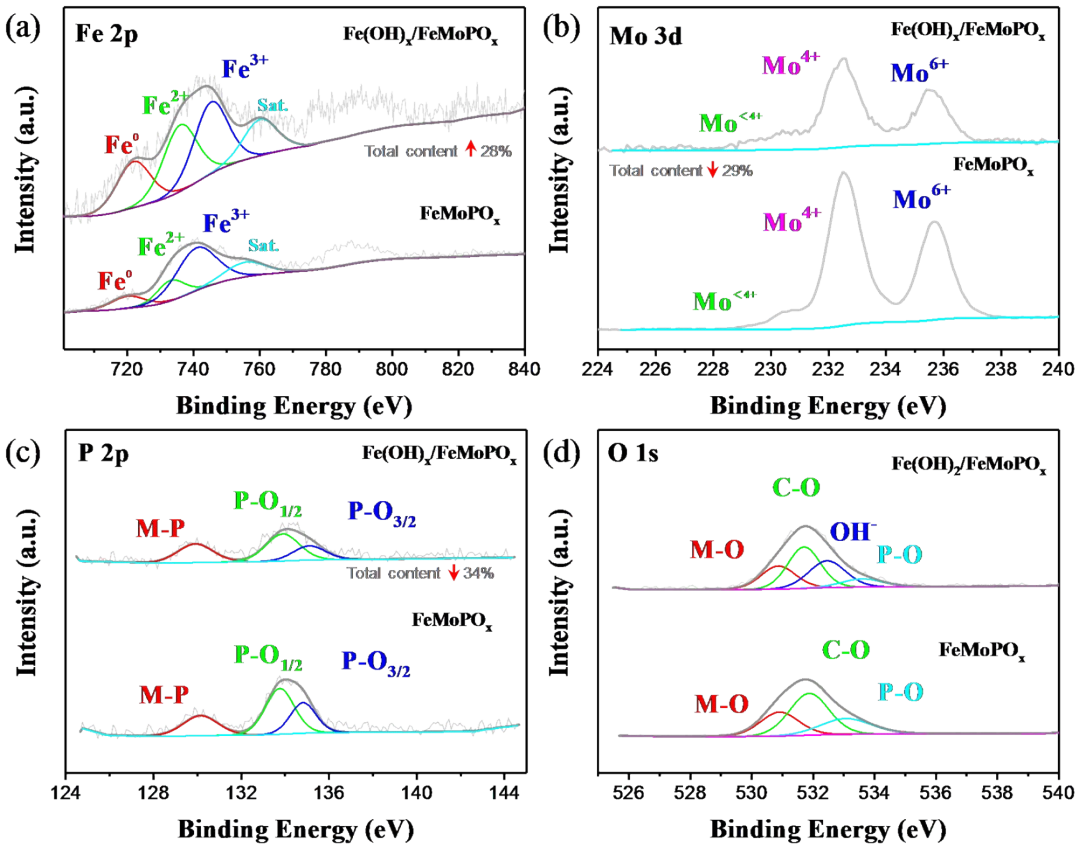

Figure S6. XPS spectra of $FeMoPO_4$, and $Fe(OH)_x/FeMoPO_x$, (a) Fe 2p region, (b) Mo 3d region, (c) P 2p region and (d) O 1s region.

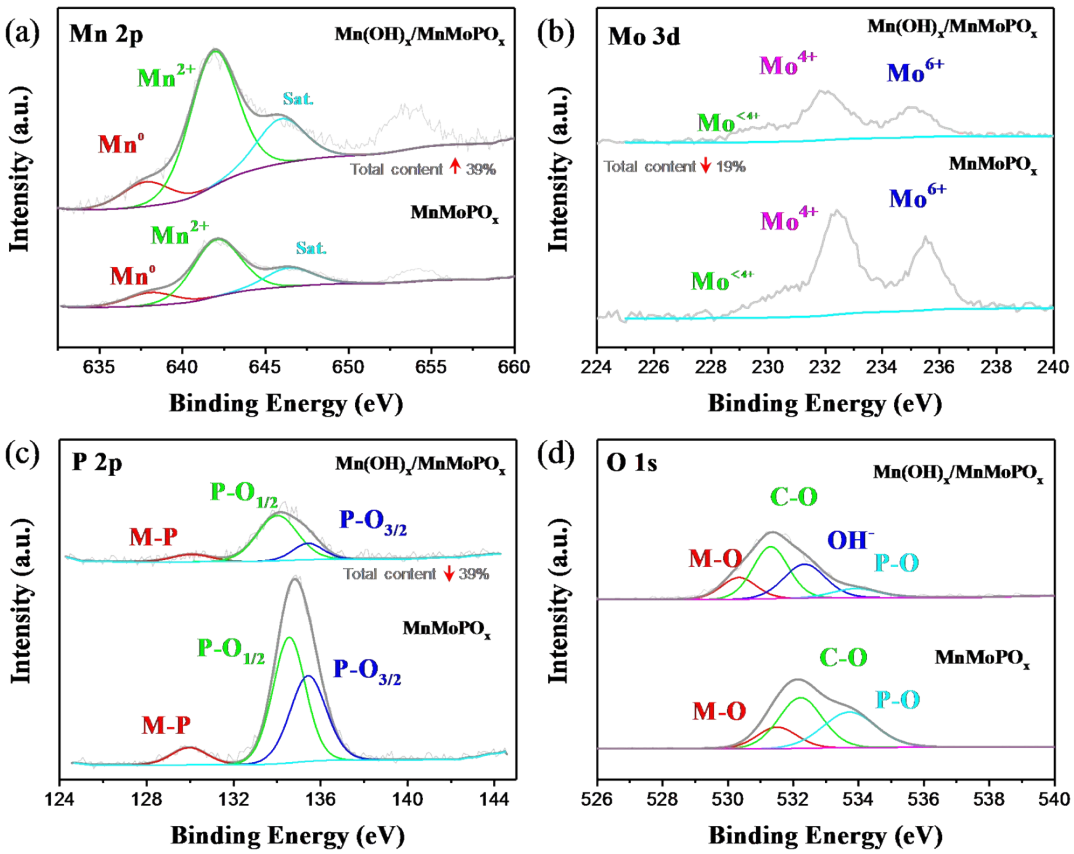

Figure S7. XPS spectra of $MnMoPO_4$, and $Mn(OH)_x/MnMoPO_x$, (a) Mn 2p region, (b) Mo 3d region, (c) P 2p region and (d) O 1s region.

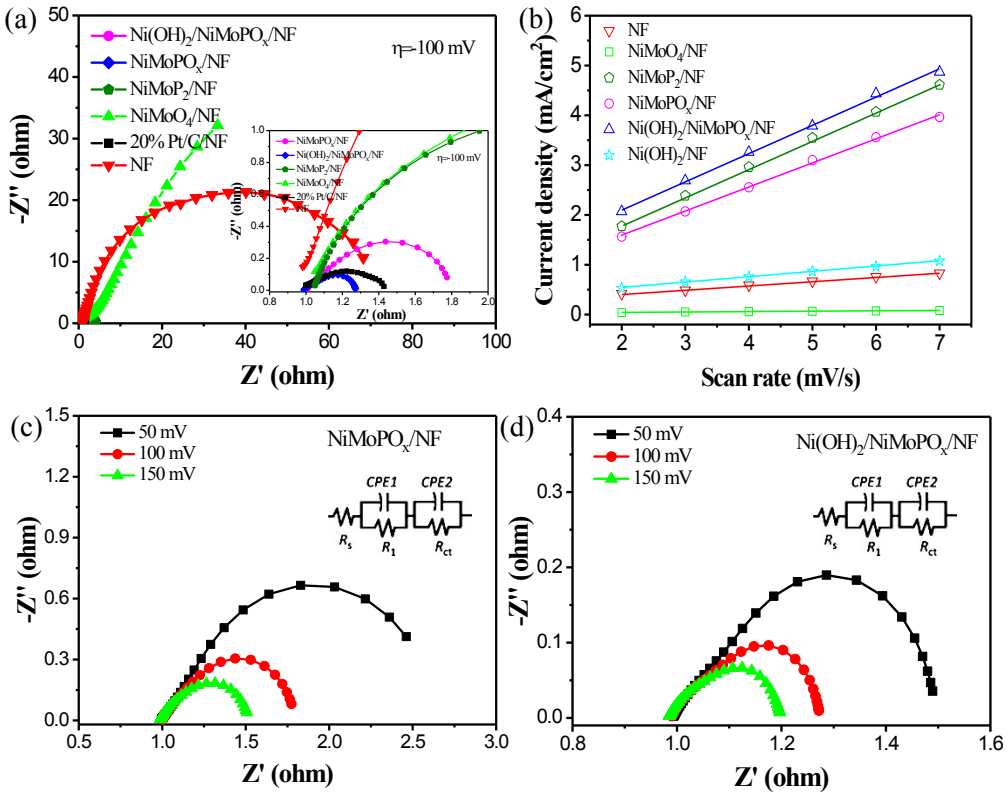

Figure S8. (a) Nyquist plots of the corresponding samples measured at a voltage of −0.1 V (vs RHE) over the frequency range 100 kHz to 0.01 Hz in 1.0 M NaOH; (b) Estimation of C_{dl} by plotting the current density variation ($\Delta j = (j_a - j_c)/2$). Nyquist plots of (c) $NiMoPO_x$/NF, (d) $Ni(OH)_2$/$NiMoPO_x$/NF measured at different voltage over the frequency range 100 kHz to 0.01 Hz in 1.0 M NaOH.

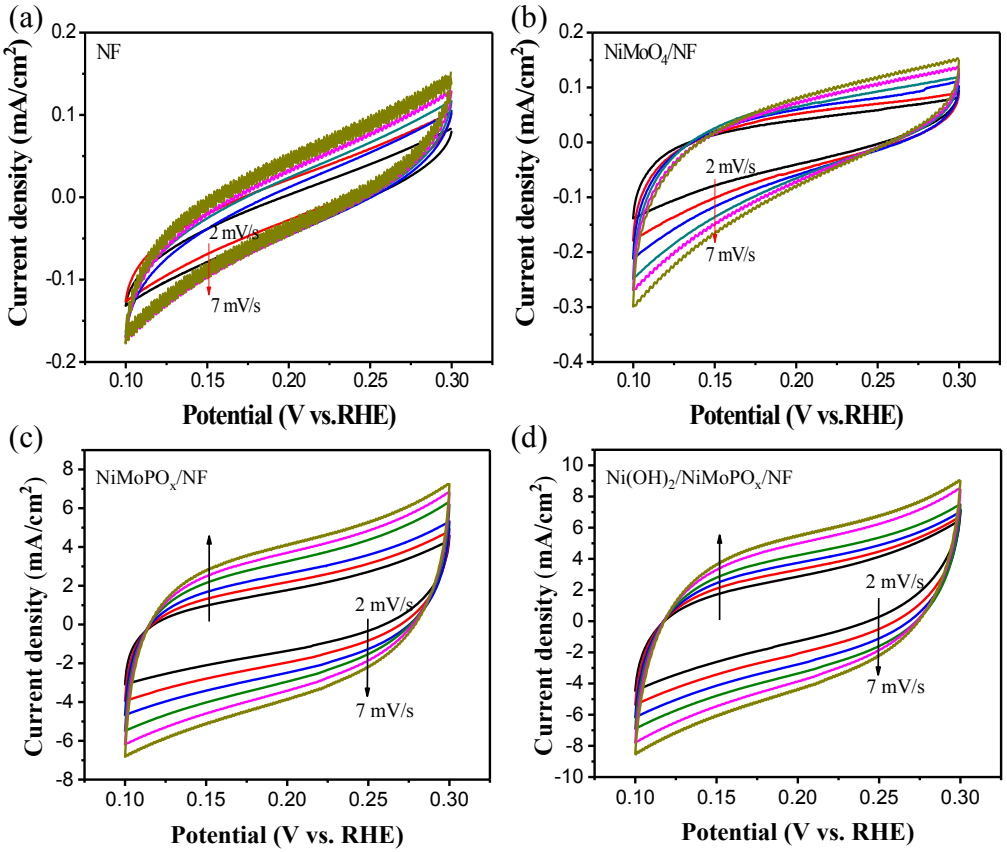

Figure S9. CVs of NF, $NiMoO_4$/NF, $NiMoPO_x$/NF, and $Ni(OH)_2$/$NiMoPO_x$/NF with various scan rates (2-7 mV/s) in the region of 0.1 to 0.3 V vs. RHE.

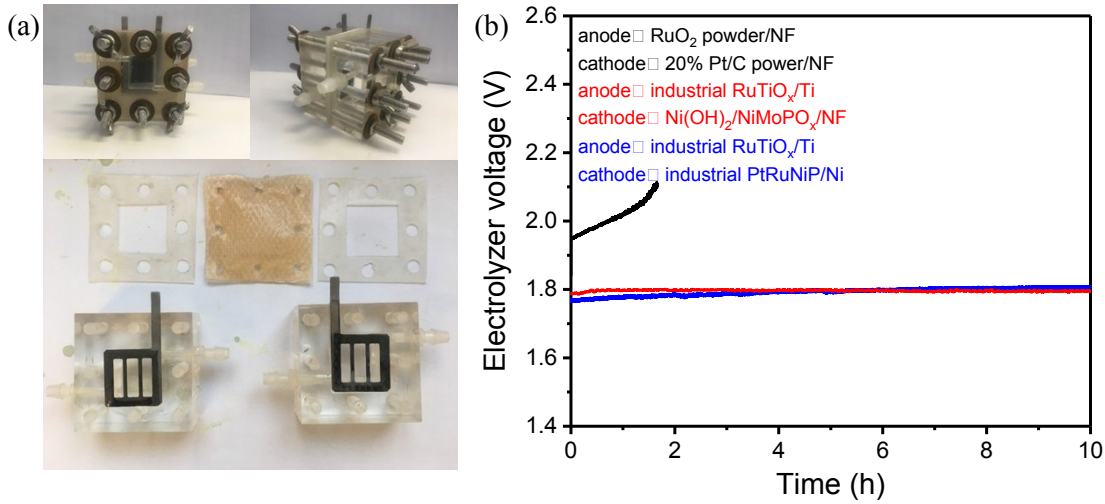

Figure S10. (a) Structure diagram of electrolyzer for water electrolysis. (b) Electrolyzer voltage at 1000 A m^{-1} of overall water electrolysis catalyzed by different catalytic electrodes in 1.0 M NaOH.

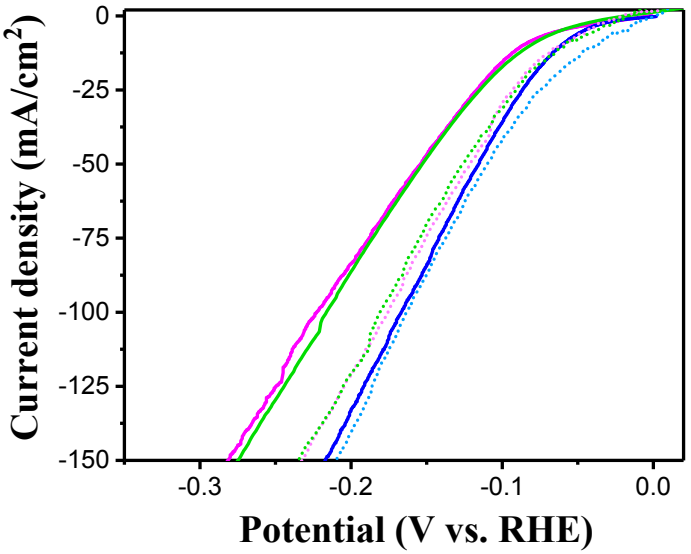

Figure S11. LSV of $NiMoPO_x$/NF, $Ni(OH)_2$/$NiMoPO_x$/NF and $Ni(OH)_2$/$NiMoPO_x$/NF-acid electrodes without iR correction.

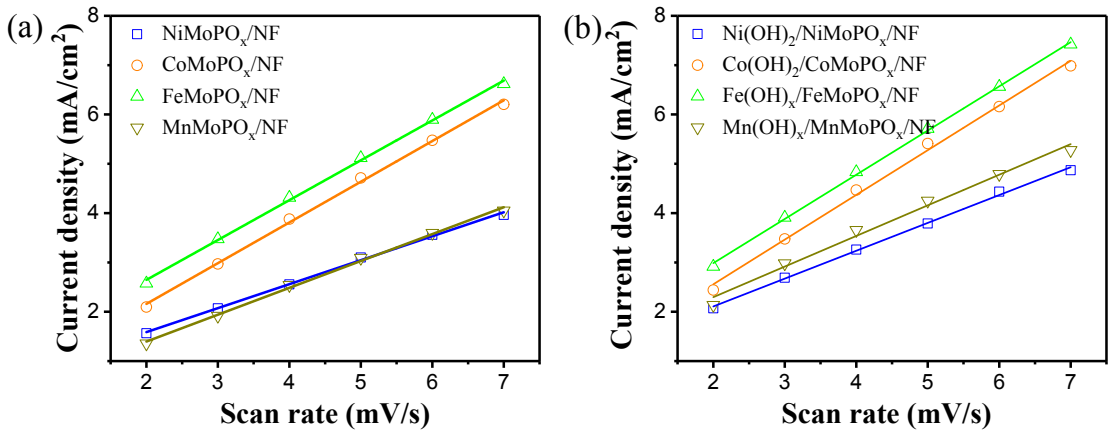

Figure S12. Estimation of C_{dl} of M(Ni, Co, Fe, Mn)-MoPO$_x$/NF (a) before and (b) after activation by plotting the current density variation ($\Delta j = (j_a - j_c)/2$).

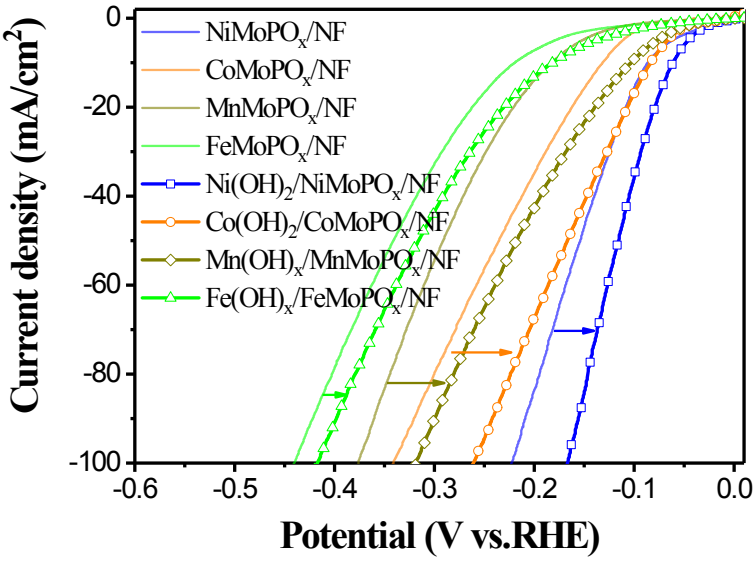

Figure S13. The ECSA-normalized HER polarization curves for $M(OH)_2$/M-$MoPO_x$/NF without iR correction (M=Ni, Co, Fe, Mn).

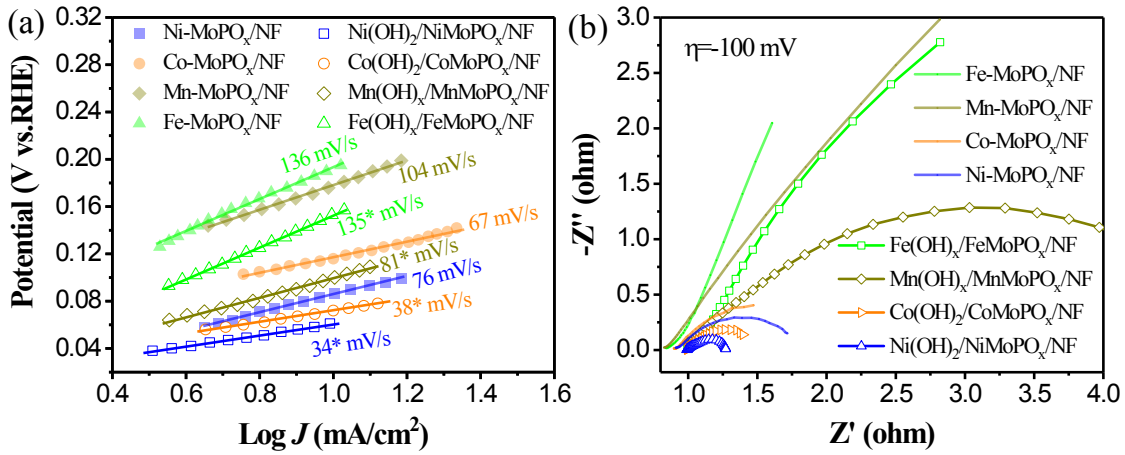

Figure S14. (a) Tafel slopes of M(Ni, Co, Fe, Mn)-$MoPO_x$/NF and their activated $M(OH)_2$/M-$MoPO_x$/NF electrodes without iR correction; (b) Nyquist plots for the corresponding samples measured at a voltage of −0.1 V (vs RHE) over the frequency range 100 kHz to 0.01 Hz in 1.0 M NaOH.

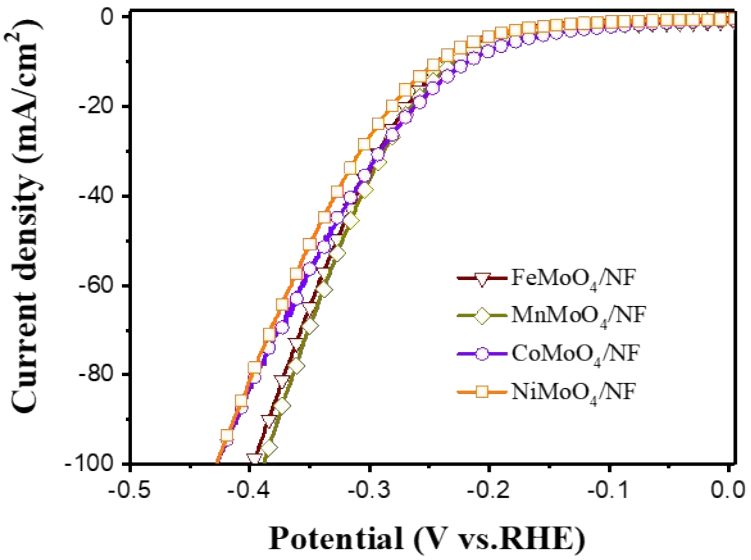

Figure S15. (a) LSV of M(Ni, Co, Fe, Mn)-MoO_4/NF precursors at 1.0 M NaOH.

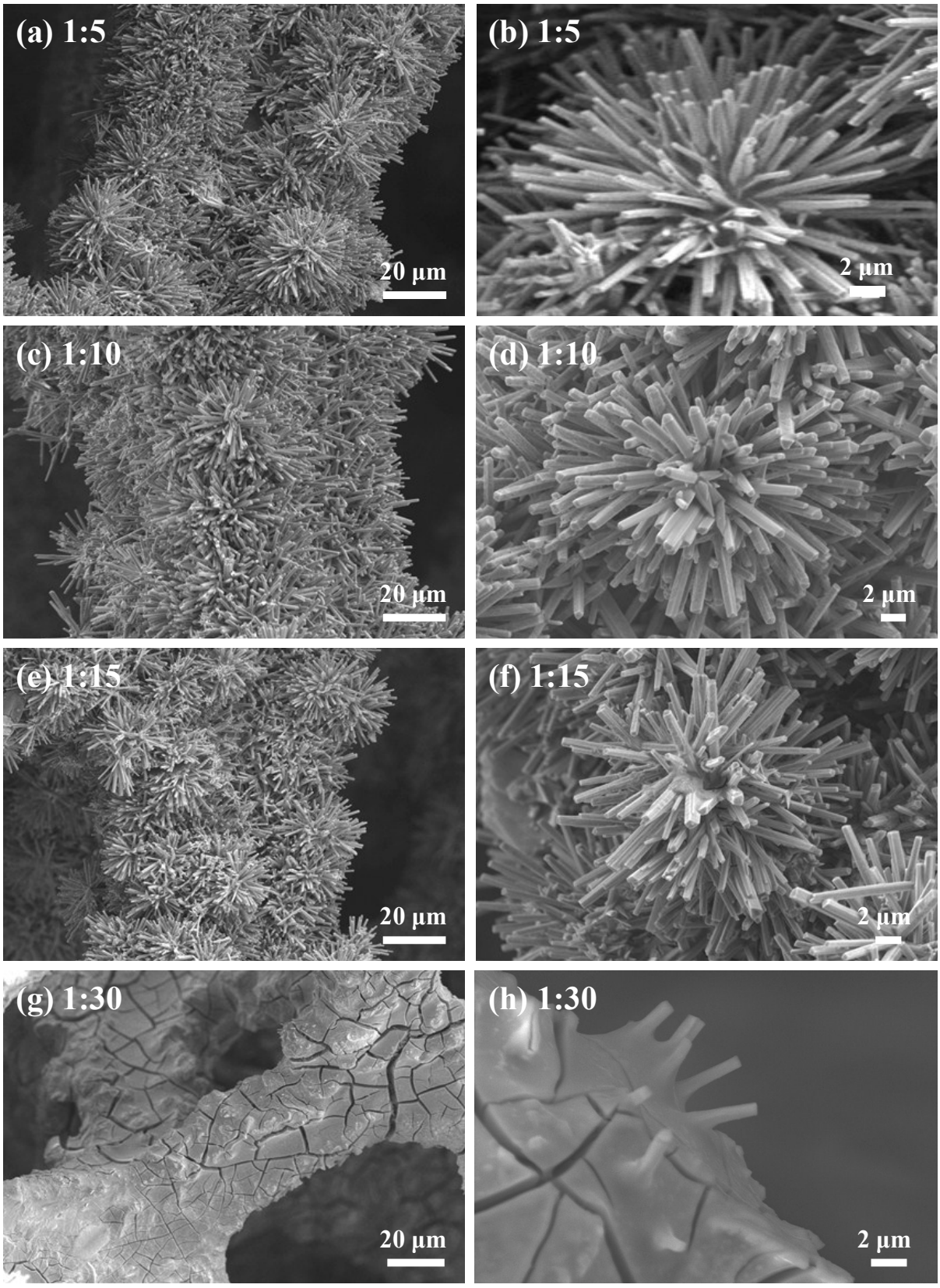

Figure S16. SEM images of $NiMoPO_x$/NF electrodes with different phosphorus sources.

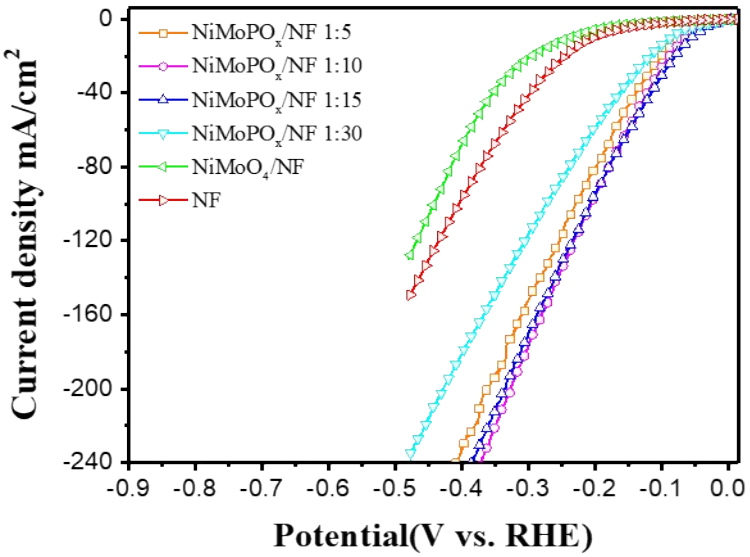

Figure S17. LSV of $NiMoPO_x$/NF prepared with different phosphorus sources at 400℃ for 2 h tested in 1.0 M NaOH.

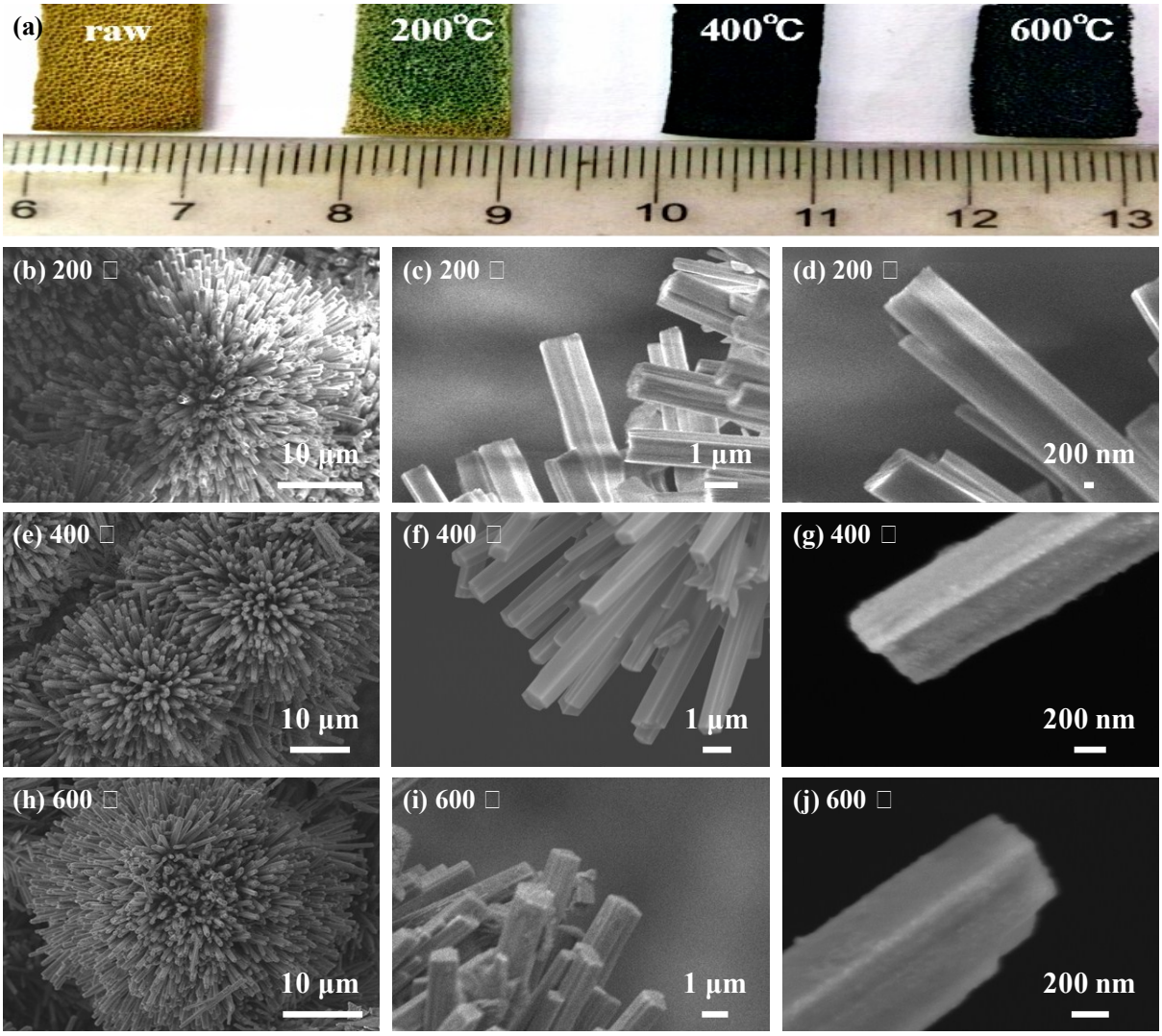

Figure S18. SEM images of $NiMoPO_x$/NF electrodes with different phosphating temperatures for 2 h.

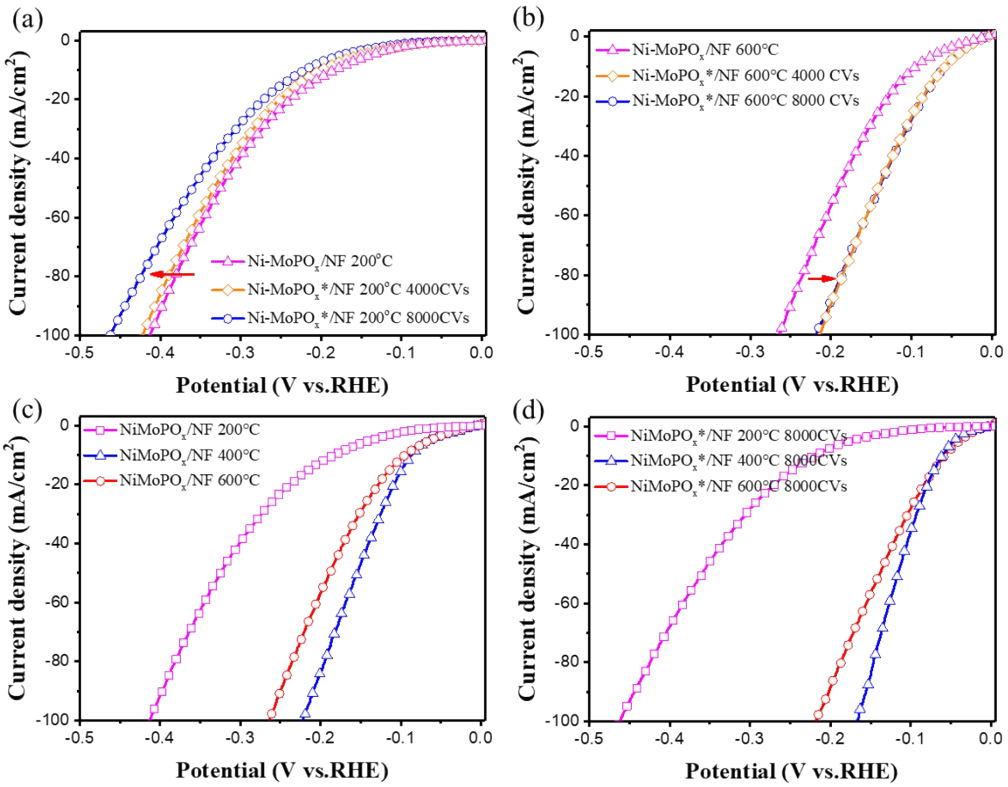

Figure S19. LSV curves of (a) NiMoPO$_x$/NF 200℃ and (b) NiMoPO$_x$/NF 600℃ activated with different CVs; LSV curves of (c) NiMoPO$_x$/NF and (d) NiMoPO$_x$*/NF with different phosphating temperature for 2 h.

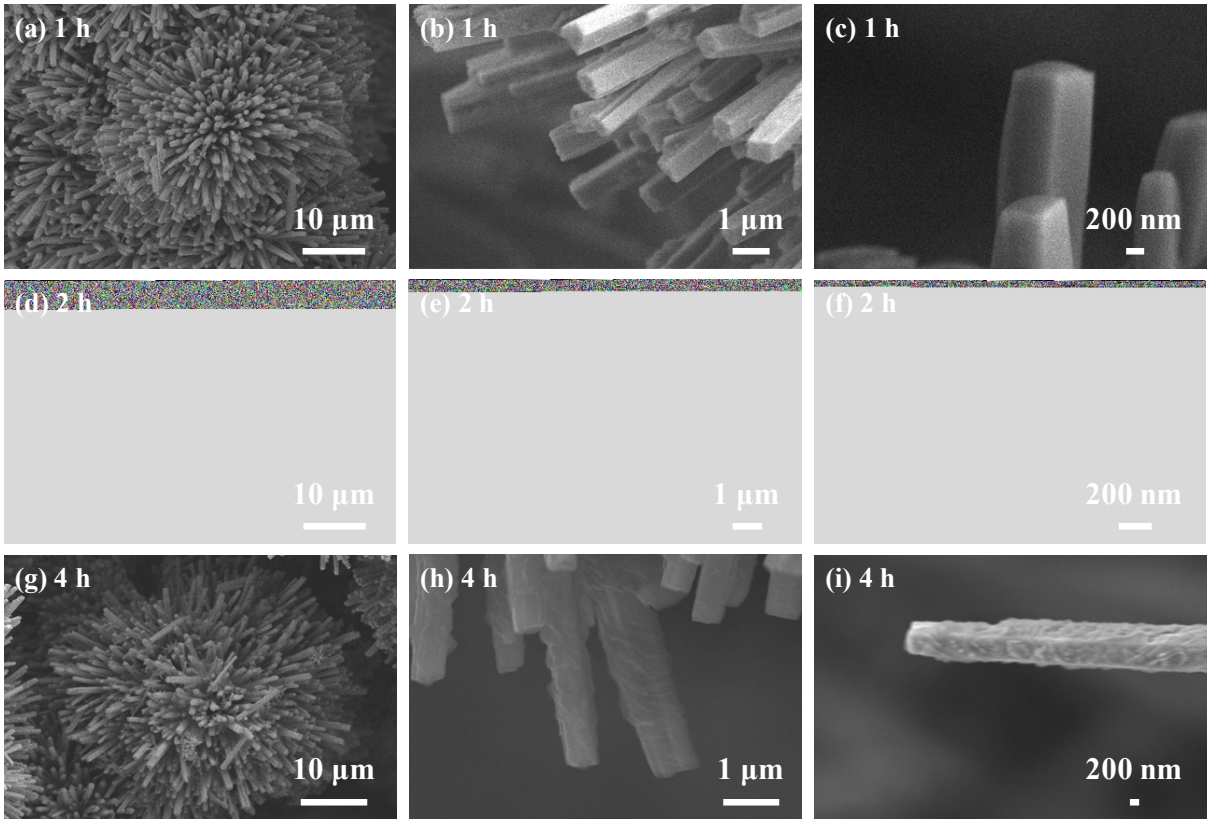

Figure S20. SEM images of $NiMoPO_x$/NF electrodes at 400℃ with different phosphating time.

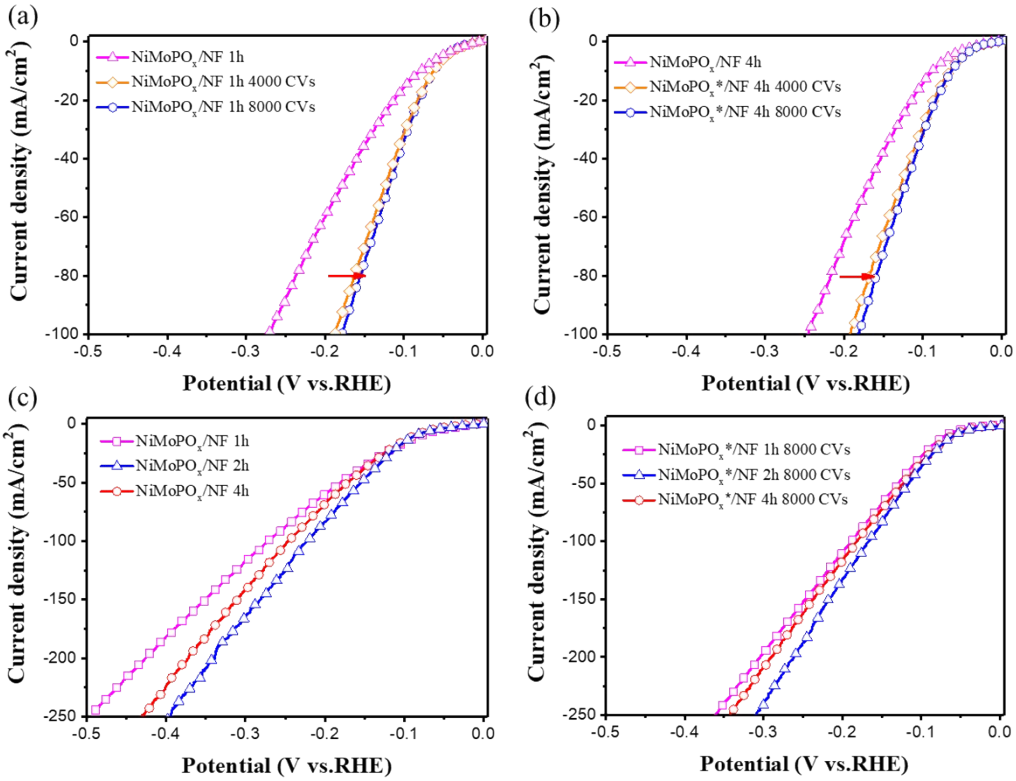

Figure S21. LSV curves of (a) NiMoPO$_x$/NF 1h and (b) NiMoPO$_x$/NF 4h activated with different CVs; LSV curves of (c) NiMoPO$_x$/NF and (d) NiMoPO$_x$*/NF with different phosphating time after 8000 CVs. All these samples were phosphatized at 400℃.

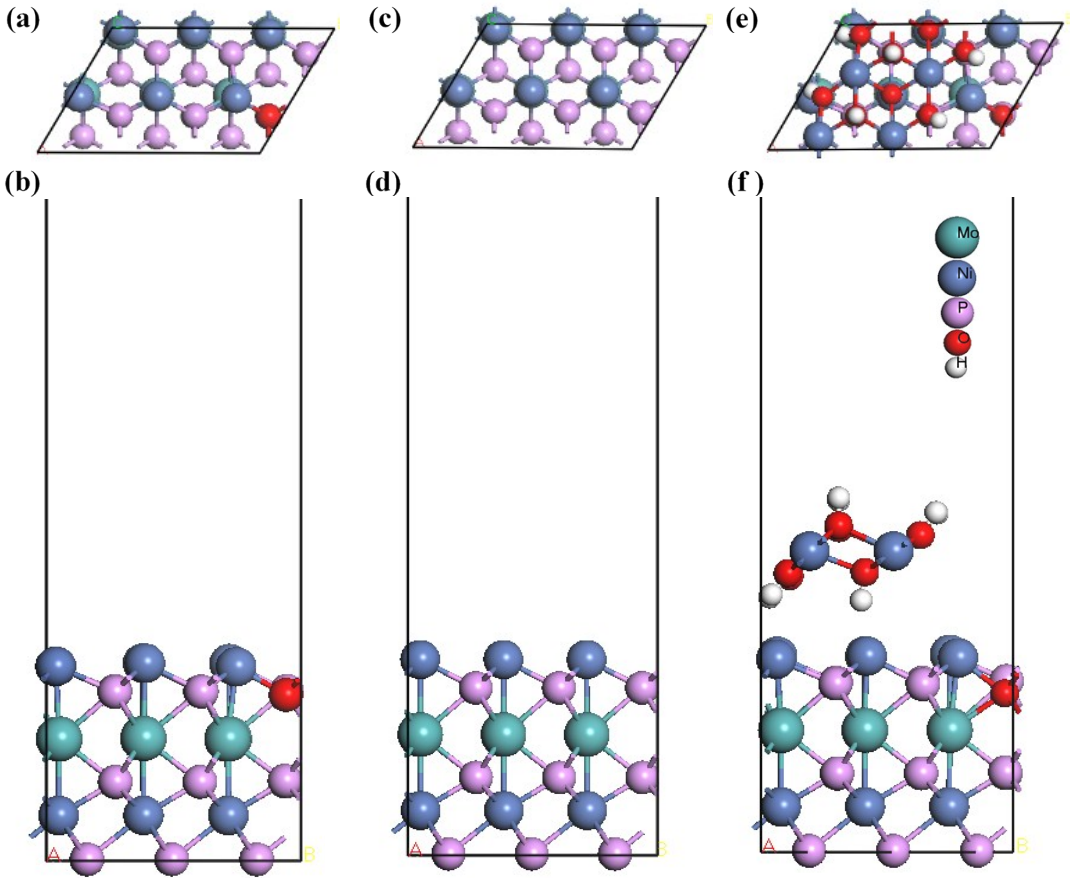

Figure S22. The (2x3) slab models of (a, b) $NiMoP_2O$, (c, d) $NiMoP_2$ and (e, f) $Ni(OH)_2/NiMoP_2O$.

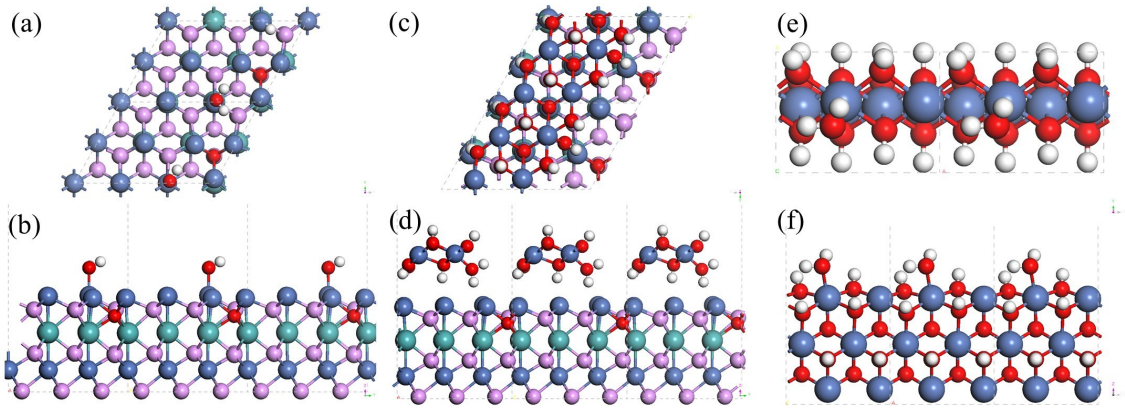

Figure S23. The (2x3) slab models of H_2O adsorbed on (a, b) $NiMoP_2O$, (c, d) $Ni(OH)_2/NiMoP_2O$ and (e, f) $Ni(OH)_2$.

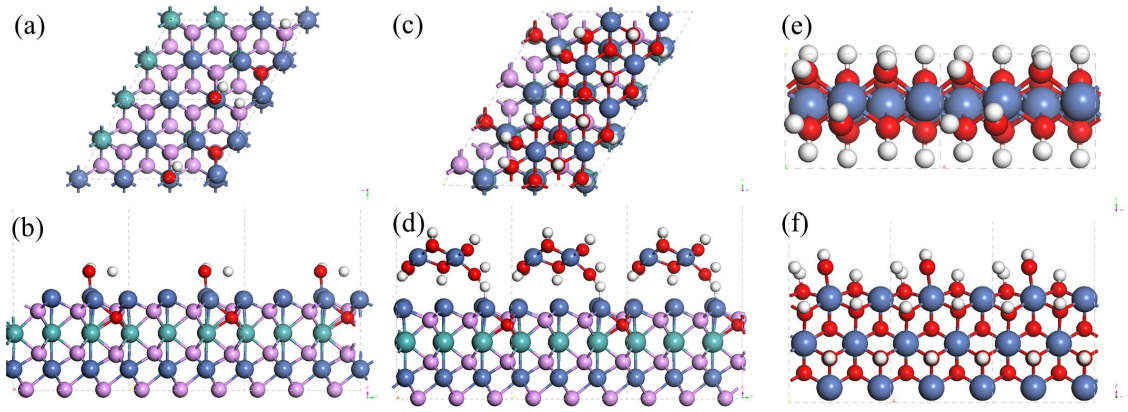

Figure S24. The (2x3) slab models of H_2O dissociated on (a, b) $NiMoP_2O$, (c, d) $Ni(OH)_2/NiMoP_2O$ and (e, f) $Ni(OH)_2$.

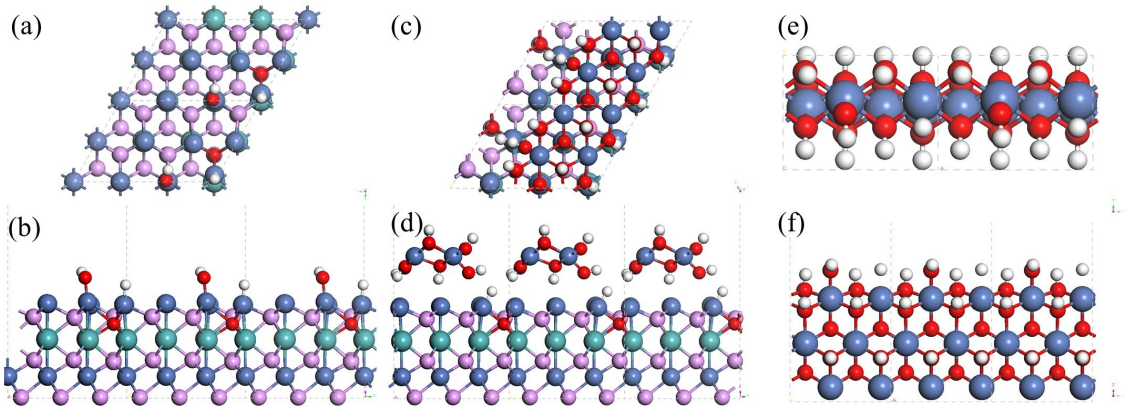

Figure S25. The (2x3) slab models of H and OH adsorbed on (a, b) $NiMoP_2O$, (c, d) $Ni(OH)_2/NiMoP_2O$ and (e, f) $Ni(OH)_2$.

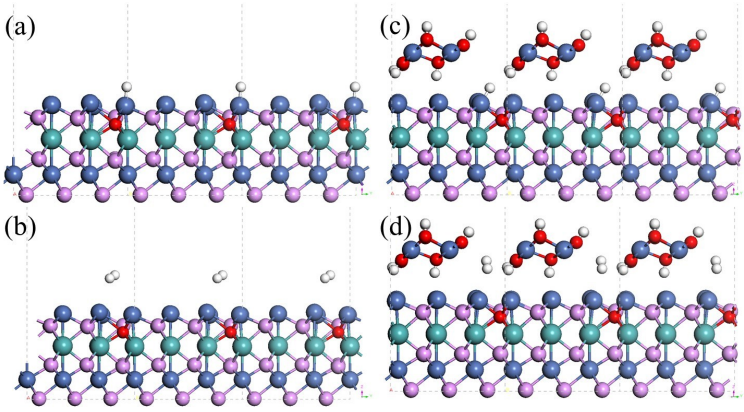

Figure S26. The (2x3) slab models of H_2 formation on (a, b) $NiMoP_2O$, (c, d) $Ni(OH)_2/NiMoP_2O$.

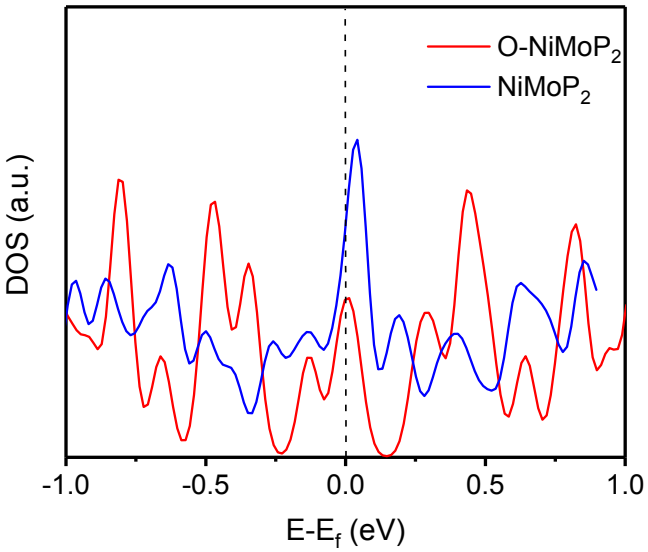

Figure S27. Calculated density of states (DOS) of the oxygen incorporated $NiMoP_2$ slab and the pristine $NiMoP_2$ slab.

Table S1. Elements contents of $NiMoPO_x$ and the activated $Ni(OH)_2/NiMoPO_x$.

Catalysts	Elements (atm %)	Ni			Mo			P		O			
$NiMoPO_x$	**Total (%)**	**9.35**			**2.87**			**19.79**		**67.99**			
	specials	Ni^0	Ni^{2+}	Ni^{3+}	$Mo^{<4+}$	Mo^{4+}	Mo^{6+}	M-P	P-O	M-O	C-O	O-H	O-P
	Content	0.12	0.51	0.37	0.08	0.43	0.49	0.04	0.96	0.41	0.40	0	0.19
$Ni(OH)_2/NiMoPO_x$	**Total (%)**	**17.57**			**2.33**			**7.26**		**72.84**			
	specials	Ni^0	Ni^{2+}	Ni^{3+}	$Mo^{<4+}$	Mo^{4+}	Mo^{6+}	M-P	P-O	M-O	C-O	O-H	O-P
	Content	0.03	0.82	0.15	0.06	0.42	0.52	0.11	0.89	0.30	0.36	0.27	0.07

Table S2. Elements contents of (Co/Fe/Mn)$MoPO_x$ and their corresponding activated hybrids.

Elements (atm %) / Catalysts	M (Co/Fe/Mn)	Mo	P	O
$CoMoPO_x$	7.63	3.37	19.04	67.96
$Co(OH)_2/CoMoPO_x$	17.82	2.87	9.58	69.72
$FeMoPO_x$	25.32	24.93	7.10	42.65
$Fe(OH)_x/FeMoPO_x$	35.22	17.58	4.68	42.52
$MnMoPO_x$	23.14	7.66	17.14	52.06
$Mn(OH)_x/MnMoPOx$	38.14	6.92	5.59	49.35

Table S3. HER performances of $NiMoO_x$/NF, $NiMoPO_x$/NF, $Ni(OH)_2$/$NiMoPO_x$/NF, 20% Pt/C/NF and NF.

Catalysts	Overpotential (mV)		Tafel slope (mV dec^{-1})	C_{dl} (mF cm^{-2})	Rct (Ω) (η= -100 mV)
	10 mA/cm^2	100 mA/cm^2			
20% Pt/C/NF	31	154	33	/	0.43
$NiMoO_4$/NF	234	328	101	0.8	162.24
$NiMoP_2$/NF	80	216	92	56.6	2.86
$NiMoPO_x$/NF	77	123	72	48.6	0.84
$Ni(OH)_2$/$NiMoPO_x$/NF	51	72	34	56.5	0.27
$Ni(OH)_2$/NF	251	396	121	10.8	>200
NF	202	314	140	8.4	72.12

Table S4. HER performances of M(Ni, Co, Fe, Mn)-$MoPO_x$/NF and their activated $M(OH)_x$/$MMoPO_x$/NF electrodes.

Catalysts / Parameters	$FeMoPO_x$/NF		$MnMoPO_x$/NF		$CoMoPO_x$/NF		$NiMoPO_x$/NF	
	-	*	-	*	-	*	-	*
Onset potential (mV)	139	75	111	49	80	38	32	29
η @ -10 mA/cm^2 (mV)	192	153	177	100	116	72	87	61
η @ -100 mA/cm^2 (mV)	370	345	360	302	258	191	222	166
Tafel slope (mV/dec)	136	135	104	81	67	38	76	34
Rct (Ω) (η= -100 mV)	19.56	8.86	13.29	6.50	1.15	0.56	0.84	0.27
C_{dl} (mF/cm^2)	80.8	89.6	54.5	62.1	82.6	90.6	48.6	56.5

Note: - means the M-$MoPO_x$/NF samples, and * means their corresponding $M(OH)_x$/$MMoPO_x$/NF samples.

Table S5. Summary of the HER performances of nonprecious materials based electrocatalysts in alkaline electrolytes reported recently.

Electrocatalysts	Electrolyte	Substrate	Loading density (mg cm^{-2})	Counter electrode	Overpotential (mV@10 mA cm^{-2})	Tafel slope (mV dec^{-1})	Reference
$Ni(OH)_2/NiMoPO_x$	1 M NaOH	Ni Foam	1.0	Carbon Rod	51	34	This work
$Co(OH)_2/CoMoPO_x$	1 M NaOH	Ni Foam	1.0	Carbon Rod	72	38	This work
CoMnCH@NF	1 M KOH	Ni Foam	5.6	Pt Wire	180	/	*J. Am. Chem. Soc.* **2017**, 139, 8320-8328.
Cu NDs/Ni_3S_2 NTs-CFs	1 M KOH	Carbon Fibers	0.52	Graphite Rod	128	76.2	*J. Am. Chem. Soc.* **2018**, 140, 610-617.
Ni-MoS_2-CC	1 M KOH	Carbon Cloth	0.89	Graphite Rod	98	60	*Energy Environ. Sci.* **2016**, *9*, 2789-2793
$NiCo_2P_x$/CF	1 M KOH	Carbon Fibers	5.9	Pt sheet	58	34.3	*Adv. Mater.* **2017**, 29, 1605502.
CoMoP@C	1 M KOH	Glassy Carbon	0.354	Graphite Rod	81	55.5	*Energy Environ. Sci.* **2017**, 10, 788-798
MoP@C	1 M KOH	Carbon	~6.0	Graphite	49	54	*Adv. Energy Mater.*

		Cloth		Rod			**2018**, 8, 1801258.
FLNPC@MoPNC/MoP-C	1 M KOH	Carbon Cloth	2.42	Carbon Rod	69	52	*Adv. Funct. Mater.* **2018**, 28, 1801527.
MoP-C	1 M KOH	Glassy Carbon	0.84	Graphite Rod	169	70	*Nano Energy* **2017**, 32, 511-519.
$MoS_2/Co(OH)_2$	1 M KOH	Glassy Carbon	0.285	Graphite Rod	125	76	*Adv. Mater.* **2018**, 30, 1801171
MoS_2 Confined $Co(OH)_2$	1 M KOH	Glassy Carbon	0.2	Graphite Rod	89	53	*ACS Nano* **2018**, 12, 4565-4573.
$Ni(OH)_2/MoS_2$	1 M KOH	Carbon Cloth	4.8	Pt Foil	80	60	*Nano Energy* **2017**, 37, 74-80

Table S6. HER performances of $NiMoPO_x$/NF and their corresponding $Ni(OH)_2$/$NiMoPO_x$/NF electrodes with different phosphating conditions.

Catalysts	$NiMoPO_x$/NF 200 ℃-2 h		$NiMoPO_x$/NF 400 ℃-2 h		$NiMoPO_x$/NF 600 ℃-2 h		$NiMoPO_x$/NF 400 ℃-1 h		$NiMoPO_x$/NF 400 ℃-4 h	
	-	*	-	*	-	*	-	*	-	*
Onset potential (mV)	94	121	32	29	45	29	45	42	40	32
η @ -10 mA/cm^2 (mV)	182	220	87	61	95	58	88	72	79	64
η @ -100 mA/cm^2 (mV)	413	462	222	166	264	218	271	189	245	183
j @-400 mV (mA/cm^2)	92	68	255	349	212	232	181	284	224	305

Note: - means the $NiMoPO_x$/NF samples, and * means their corresponding $Ni(OH)_2$/$NiMoPO_x$/NF samples.